Journal of Applied Polymer Science

# Enhanced dielectric and electrorheological properties of needle-like $TiO_2$/polyrhodanine core/shell hybrid nanostructure

**Seyma Ozkan, Halil Ibrahim Unal**
Smart Materials Research Lab., Department of Chemistry, Faculty of Science, University of Gazi, Ankara, Turkey
Correspondence to: H. I. Unal (E-mail: hiunal@gazi.edu.tr)

**ABSTRACT:** In this study, antisedimentation, dielectric, electrorheological (ER) and creep–recovery properties of needle-like $TiO_2$/polyrhodanine (PRh) nanocomposite were investigated. Antisedimentation ratio of needle-like $TiO_2$/PRh was determined to be 45% after 30 days in silicone oil (SO). Polarizability and relaxation time of needle-like $TiO_2$/PRh/SO system were determined to be 0.18 and $2.9 \times 10^{-5}$ s, respectively by the dielectric spectroscopy which was further used to evaluate the ER performance of the dispersion, and the data obtained were in good agreement with the overall ER results. ER properties of needle-like $TiO_2$/PRh/SO system were determined by taking the effects of shear rate, shear stress, electric field strength, and temperature into account using a torque electrorheometer. Non-Newtonian shear thinning behaviors were observed for the samples. Vibration damping capabilities of the dispersions were investigated by measuring their elastic and viscous moduli as functions of frequency, time, and electric field strengths. Enhanced and reversible viscoelastic deformations were recorded for needle-like $TiO_2$/SO system from creep–recovery tests with 88% recovery under $E = 3.5$ kV mm$^{-1}$ condition; thus, the system was classified as a smart one and suitable for potential vibration damping applications. © 2015 Wiley Periodicals, Inc. J. Appl. Polym. Sci. **2016**, *133*, 43240.

**KEYWORDS:** conducting polymers; dielectric properties; nanostructured polymers; rheology; viscosity and viscoelasticity

Received 8 October 2015; accepted 17 November 2015
**DOI: 10.1002/app.43240**

## INTRODUCTION

$TiO_2$ is one of the most widely used inorganic industrial material.[1] It has found applications in glasses, ceramics, cosmetics, sun blinds, papers, drugs, paints, foods, plastics, and fibers due to its high refractive index and resistance to the UV light. Beside its pigment property, $TiO_2$ is also widely used in photocatalysis, gas sensors, Li-ion batteries, medical applications, and antimicrobial coatings. $TiO_2$ is also an important material from technical point of view and it has three crystalline structures namely anatase, rutile and brookite. While the crystalline structure of anatase and rutyl is tetragonal, brookite has orthorhombic.[2,3] These unique properties of $TiO_2$ can be improved by altering the surface chemistry of $TiO_2$ nanoparticles by various surface functionalization techniques by applying bottom-up or up-bottom engineering strategy.[4]

Crystallinity, particle size, and surface properties depend on the fabrication process of $TiO_2$. Mainly sol–gel, hydrothermal, and electrochemical oxidation techniques are applied to produce nanometer sized $TiO_2$ particles with desired chemical and physical properties. However, these nanoparticles often have a tendency to agglomerate which limits both their size-related advantageous and the ability to assemble them into a chosen structural arrangement under various external stimulus, such as magnetic and/or electric field strengths, which greatly influence the dispersions' magnetorheological and/or electrorheological behavior.[5] To try to minimize these shortcomings, nanoparticles are usually surface functionalized to improve handling which involves bottom-up surface engineering approach to form core/shell structures by covering the surfaces of $TiO_2$ particles by long-chain organic molecules, such as polyrhodanine.[6]

These inorganic/organic hybrid nano materials expose unique mechanical, electrical, optical, chemical, colloidal, and rheological properties. One of the main shortcomings of these hybrid materials are their colloidal instabilities which is a very important parameter for potential industrial applications. If the van der Waals type attractive forces are dominant the colloidal dispersion will be unstable whereas, if the electrostatic repulsions are dominant it well remain unsettled which is clearly explained in the DLVO theory.[7] The magnitude of these forces in other words colloidal stability of dispersion may be altered by adding same or oppositely charged particles into the dispersion medium.

To enhance the colloidal stability of a dispersion, various inorganic-core/conducting polymer–shell structured hybrid materials have been prepared. These materials are also used as dispersing phase in ER fluids and attracted many scientific and technological researches.[8,9] Shape, size, and morphologies of inorganic core

materials and type and thickness of conducting polymer shell can be engineered in a controllable way to enhance the colloidal stability of a dispersion and to observe high ER activity.[10] Several high ER active materials are reported recently by Shen *et al.* based on polar molecule dominated ER dispersion[11] and by Wu *et al.*, based on $SiO_2$–titanium oxalate and $TiO_2$–titanium oxalate hybrid particles and especially the influence of high dielectric constant core on the ER activity of core/shell structured hybrid materials are discussed.[12]

Dielectric materials with high dielectric constants, low dielectric losses, and high energy storage capabilities find applications in electroactive systems, capacitors, dielectric resonators, field-effect transistors, industrial coatings, mineral oils, and especially in ER fluids.[13,14] Traditional inorganic core materials, such as $TiO_2$, $BaTiO_3$, $CaTiO_3$, have high value of dielectric constants. In pristine form they show low ER activities. To enhance their ER performances, their surfaces can be modified by covering with conducting polymer shells by surface initiated polymerization. In this method initiator, such as $FeCl_3$ is firstly bounded to the surfaces of inorganic nanoparticles and then monomer is polymerized at the surfaces of inorganic particles to obtain engineered materials with core–shell structure. By this method, dielectric, conductivity, density, and colloidal stabilities of new hybrid materials can be enhanced when compared to the nonmodified ones and show longer shelf lives.[15]

Core–shell structured hybrid nanoparticles with desired dielectric properties are used widely in the ER fluids. A typical type of ER fluid is a colloidal suspension of polarizable solid dielectric or semi conducting particles dispersed in an insulating fluid, which often exhibits Newtonian fluid behavior in the absence of an applied electric field. This fluid became polarized immediately when an external electric field strength is applied and the dispersed particles align along the direction of the electric field anisotropically, resulting in increased shear viscosity and shear stress by showing a yield stress. Therefore, the rheological flow behavior of the ER fluid can usually be explained by the Bingham fluid model with the yield stress.[16] Since the first discovery of ER fluids, dielectric materials have triggered enormous amount of research activity both in theory[17] and in the development of various engineering applications, such as shock absorbers,[18] engine mounts and smart reversible vibration damping structures with suitable viscoelastic properties and long-term use.[19,20]

The time dependent increase in strain ($\gamma$) under stress ($\tau$) and recovery after the removal of stress is defined as creep–recovery. By this experiment it is possible to obtain information on the viscoelastic properties, time dependent deformations, reusability of ER active materials in industrial applications; and also to get insight into the intermolecular interactions of electric field stimuli oriented molecules, which influence the mobility of molecules and the mechanistic origin of the flow of a material under time, stress, temperature, and frequency dependent deformations. In addition, relaxation, or retardation spectra of oriented molecules can be calculated from the creep–recovery experiments.[21] It was noticed that there are limited number of reports on the creep–recovery behaviors of core/shell structured hybrid ER active materials.[22,23] By monitoring the creep and recovery behavior of ER fluids at various stress levels, viscoelastic properties of needle-like $TiO_2$/SO, and needle-like $TiO_2$/PRh/SO systems were identified in this study.

To the best of our knowledge, antisedimentation, dielectric, electrorheological, creep–recovery, and vibration damping characteristics of needle-like $TiO_2$/PRh nanocomposite is not hitherto been reported in the literature. In this study, ER properties of needle-like $TiO_2$ and needle-like $TiO_2$/PRh nanoparticles were investigated and their viscoelastic properties were examined by creep and creep–recovery tests. The first part of this study was focused on the synthesis, structural, thermal, morphological, and surface characterizations, electrokinetic properties, and antibacterial characteristics.[2] Furthermore, from this point of view, a new, an inexpensive raw material composed of needle-like $TiO_2$ and PRh chains is believed to increase the number of scientific investigations as an attractive substitute between the antibacterial ER active fluids.

## EXPERIMENTAL

### Materials

All the chemicals were provided from Sigma (Germany) and used as received. Rutile type needle-like $TiO_2$ was purchased from Nanostructured and Amorphous Materials. The densities of $TiO_2$ and $TiO_2$/PRh particles were 0.297 and 0.265 g $cm^{-3}$, respectively. Density and viscosity of silicone oil used for dielectric and ER measurements were 0.97 g $cm^{-3}$ and 200 mPa s, respectively, and viscosity of silicone oil used for antisedimentation measurement was 5 mPa s.

### Synthesis of Needle-Like $TiO_2$/Polyrhodanine Core/Shell Nanocomposite

Facile synthesis of core/shell structured rutile type needle-like $TiO_2$/polyrhodanine nanocomposite was carried out by using $FeCl_3$ as the oxidant and taking the mole ratio of $TiO_2$:$FeCl_3$ as 1:1. Full details of the reaction procedure, all the characterization data and antibacterial properties were given in our previous publication.[2] The homogeneously distributed shell thickness of PRh chains on the surfaces of needle-like $TiO_2$ was between 4.8–6.5 nm and the conductivity of needle-like $TiO_2$/PRh nanocomposite was $1.8 \times 10^{-5}$ S $cm^{-1}$.[2]

### Characterizations

**Preparation of Suspensions.** Suspensions of needle-like $TiO_2$ and needle-like $TiO_2$/PRh nanocomposite were prepared in SO at the volume fraction of $\varphi = 2.5$ V/V%, by dispersing definite amount of solid particles in SO which were both vacuum dried before mixing in an oven for overnight to remove any redisual moisture.

**Antisedimentation Ratio Measurements.** Antisedimentation ratio was defined as the height of the particle-rich phase divided to the total height of dispersion as indicated in the inset of Figure 1. Antisedimentation stabilities against gravitational forces of the needle-like $TiO_2$/SO and needle-like $TiO_2$/PRh/SO dispersions were determined to characterize the suspended stabilities of the ER fluids. Graduated flasks containing the above mentioned dispersions were immersed into a constant temperature ($25 \pm 0.1$°C) water bath and formations of the first precipitates were recorded to be the indication of colloidal

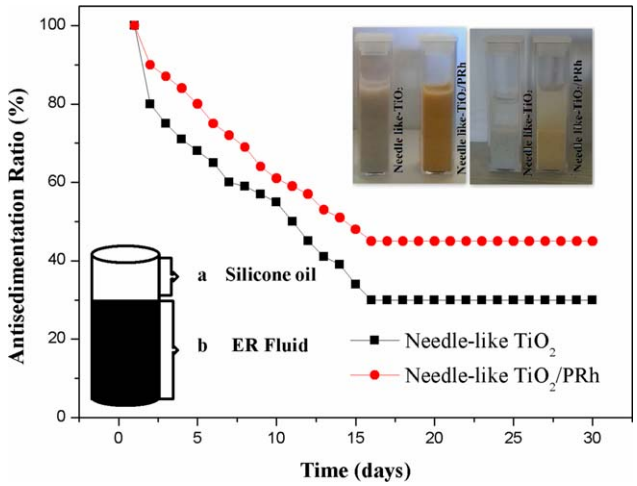


**Figure 1.** Antisedimentation stability results of the suspensions ($\varphi = 2.5\%$, $T = 25°C$). [Color figure can be viewed in the online issue, which is available at wileyonlinelibrary.com.]

instability. During the neat eye observations, the height of phase separation between the particle-rich phase and the relatively clear oil-rich phase was recorded as a function of time by using a digital composing stick.

**Dielectric Constant Measurements.** Dielectric constants of needle-like $TiO_2$/SO and needle-like $TiO_2$/PRh/SO systems were measured at a frequency range of 20 Hz-2 MHz using Agilent E4980A Precision model impedans analyzer/LCR Meter (Agilent) adapted with 16452A model liquid test fixture at constant conditions of $T = 25°C$, $V = 1.0$ V (AC), and $C_p$–$R_p$ mode.

**Electrorheogical Measurements.** ER properties of the dispersions were measured with a Termo-Haake RS600 parallel plate torque electrorheometer (Germany). The gap between the 35 mm parallel plates was 1.0 mm. Shear rate–shear stress–viscosity curves were obtained under the controlled rate (CR) mode within the shear rate range of 0.01–1500 $s^{-1}$ by maintaining the samples for 30 s to let the equilibrium structure form. The collected data were evaluated by using the Rheowin software. The potential used in these experiments was supplied by a 0–3.5 kV (with 0.5 kV increments) DC electric field generator (Fug Electronics, HCL 14), which enabled resistivity to be created during the experiments.

**Creep and Creep–Recovery Measurements.** During the creep–recovery experiment, external stresses of $\tau_0 = 10$, 20, 30 Pa were applied instantaneously ($t = 100$ s) onto the needle-like $TiO_2$/PRh/SO suspensions and changes in their strains ($\gamma$) were measured over a period of time. Then the stress was set to $\tau_0 = 0$ Pa to determine the recoverable elastic portion of the deformation.

## RESULTS AND DISCUSSION

### Antisedimentation Stability Results

Antisedimentation stability of an ER material is one of the main criteria to evaluate whether the suspended particles remain homogeneously dispersed in a stationary phase of a suspension before applying external electric field strength; so that stable electric field induced fibrillar structures are formed. It is well known that the ER effect dramatically decreases as the sedimentation of suspended particles increase. The most important factors affecting the colloidal stability of dispersions are density mismatch and wettability of the dispersed and continuous phases. Antisedimentation stability can be enhanced by controlling size, shape, and surface roughness of the dispersed particles, and selecting the dispersant medium with a closer density to the particles. As reflected from Figure 1, antisedimentation ratios of needle-like $TiO_2$/SO and needle-like $TiO_2$/PRh/SO systems decreased to 30 and 45% after 16 days and then levelled off during the rest of the observations and indicating that core/shell structured hybrid nanocomposite became more resistant against gravitational forces after covering with PRh shells as targeted. The higher the antisedimentation ratio the better the suspended stability was. In a study carried out on pristine $TiO_2$, $TiO_2$–titanium oxalate and $SiO_2$–titanium oxalate antisedimentation stabilities were reported to be 87.5, 92.1, and 93.8%, respectively by Wu *et al.* and these high colloidal stabilities were attributed to high dielectric constant values of the core materials in the core/shell structured nanocomposites.[12] In another study carried out in our laboratory, antisedimentation stabilities of nanosphere–$TiO_2$/SO and nanosphere–$TiO_2$/PPy/SO systems were determined to be 15 and 54%, respectively. It was concluded that spherical particles are less resistive against gravitational forces and after forming a core/shell structure colloidal stabilities of pristine inorganic particles were successfully enhanced.[24]

### Dielectric Constant Results

To prepare high performance ER fluids, dielectric properties of dispersed particles need to be determined before ER measurements to be carried out. For this purpose dielectric spectra of needle-like $TiO_2$/SO and needle-like $TiO_2$/PRh/SO dispersion systems were investigated by using an LCR meter equipped with a liquid test fixture and dielectric data were calculated using the following equations[25]:

$$\varepsilon_r = \frac{\varepsilon}{\varepsilon_o} \tag{1}$$

$$\varepsilon_r = \varepsilon_r' - i\varepsilon_r'' \tag{2}$$

$$\varepsilon_r' = \frac{dC_p}{A\varepsilon_0} \tag{3}$$

$$\varepsilon_r'' = \frac{dC_p}{\omega R_p A\varepsilon_0} \tag{4}$$

where $C_p$ is capacitance, $d$ is distance between the electrodes, $A$ is electrode area, $\omega$ is angular frequency ($2\pi f$), and $R_p$ is resistance. Dielectric spectra of the dispersions are depicted in Figure 2. These experimental curves are also fitted by using Cole–Cole equation.[25]

$$\varepsilon^* = \varepsilon' + i\varepsilon'' = \varepsilon_\infty + \frac{\varepsilon_0 - \varepsilon_\infty}{(1 + i\omega\lambda)^{1-\alpha}} \tag{5}$$

The real ($\varepsilon'$) and imaginary ($\varepsilon''$) components of the complex dielectric constant ($\varepsilon^*$) as a function of frequency is expressed as follows:

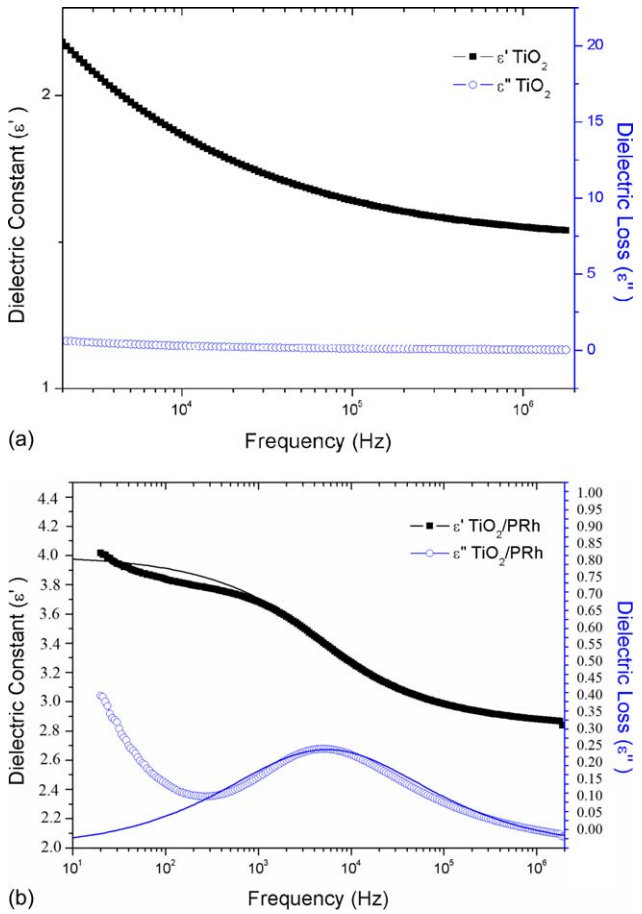


**Figure 2.** Dielectric spectra of needle-like $TiO_2$/SO and needle-like $TiO_2$/PRh/SO suspensions. Solid lines show Cole–Cole curve fittings ($\varphi = 2.5\%$). [Color figure can be viewed in the online issue, which is available at wileyonlinelibrary.com.]

$$\varepsilon' = \varepsilon_\infty + \frac{(\varepsilon_0 - \varepsilon_\infty)\left[1 + (\omega\lambda)^{1-\alpha} sin\frac{\alpha\pi}{2}\right)}{1 + 2(\omega\lambda)^{1-\alpha} sin\frac{\alpha\pi}{2} + (\omega\lambda)^{2(1-\alpha)}} \quad (6)$$

$$\varepsilon'' = \frac{(\varepsilon_0 - \varepsilon_\infty)(\omega\lambda)^{1-\alpha} cos\frac{\alpha\pi}{2}}{1 + 2(\omega\lambda)^{1-\alpha} sin\frac{\alpha\pi}{2} + (\omega\lambda)^{2(1-\alpha)}} \quad (7)$$

where $\varepsilon'$ is dielectric constant, $\varepsilon''$ is dielectric loss, $\varepsilon_0$ is static dielectric constant ($f \to 0$), $\varepsilon_\infty$ is infinite dielectric constant ($f \to \infty$), $\lambda$ is dielectric relaxation time ($1/2\pi f_{max}$), $(1 - \alpha)$ is distribution of relaxation time ($0 \leq \alpha < 1$).

Interfacial polarization relaxation time ($\lambda$) and polarizability ($\Delta\varepsilon = \varepsilon_0 - \varepsilon_\infty$) parameters of Cole–Cole equations are related to shear stress and yield stress of ER fluids. Relaxation time is inversely proportional to the polarization rate and $\Delta\varepsilon$ shows polarizability and also related to the electrostatic interactions between the dispersed particles. From the dielectic spectra, no polarizability ($\Delta\varepsilon$) and relaxation peaks ($\lambda$) were observed for the pristine needle-like $TiO_2$ but dielectric spectra were recorded after fabricating the core/shell structured needle-like $TiO_2$/PRh and the following data were obtained (Figure 2): $\varepsilon_0$: 4, $\varepsilon_\infty$: 2.82, $\Delta\varepsilon$: 0.18, $\lambda$: $2.9 \times 10^{-5}$, $\alpha$: 0.455. The enhanced dielectric data of needle-like $TiO_2$/PRh hybrid nanoparticles may be attributed to the enhanced conductivity after covering of surfaces of the needle-like $TiO_2$ particles with PRh chains. Relaxation times determined for needle-like $TiO_2$/PRh indicated that relaxation times were shortened and highly polarisable particles with enhanced mobilities were ready to act as suspended ER particles and form stiffer electric field induced anisotropic structures with enhanced electric field induced viscosities. This result is in accordance with the study reported by Wei *et al.*, on mesoporous–$TiO_2$/polypyrrole (PPy) system.[26] It was also reported in the literature that for a good ER active material, its relaxation frequency needs to be between $10^2$ and $10^5$ Hz.[27] In conclusion, dielectric measurements showed that needle-like $TiO_2$/PRh particles were good candidates as dispersed phases for ER active fluids. It was reported in a study carried out on pristine $TiO_2$, $TiO_2$–titanium oxalate and $SiO_2$–titanium oxalate, their dielectric properties were enhanced after forming core/shell structured nanocomposites and positively affected the resultant ER performance.[12] In another study carried out in our research group on pristine nanosphere–$TiO_2$ and covalently bonded nanosphere–$TiO_2$/PPy; $\Delta\varepsilon_{nanosphere-TiO2} = 0.173$, $\lambda_{nanosphere-TiO2} = 2.2 \times 10^{-5}$, $\Delta\varepsilon_{nanosphere-TiO2/PPy} = 0.170$, $\lambda_{nanosphehere-TiO2/PPy} = 1 \times 10^{-5}$ were determined. It was concluded that polarizabilities and relaxation times of $TiO_2$ nanoparticles depend on their geometries as well as nature of the shell material used to cover their surfaces.[24]

## ELECTRORHEOLOGICAL RESULTS

### Determination of ER Response Times

Determination of the responses to the external electric field stimulus and reproducibility of ER structure formed by needle-like $TiO_2$/SO and needle-like $TiO_2$/PRh/SO systems are important parameters for potential industrial applications. For this purpose, changes of shear stresses with time under varying electric field strengts were measured (Figure 3) to determine whether the same magnitude of responses can be achieved by switching the electric field on and off. During these experiments $E = 0 - 3.5$ kV mm$^{-1}$ were applied to the suspensions (with $E = 0.5$ kV mm$^{-1}$ increments) for 30 s and electric field induced shear stresses were measured; then electric field strength was set to $E = 0.0$ kV mm$^{-1}$ and waited for 30 s for the system to return to its initial level. When $E \neq 0$ kV mm$^{-1}$, shear stresses of the materials increased suddenly, whereas when $E = 0$ kV mm$^{-1}$, they sharply declined to their initial level. It was observed that the transformation of the shear stresses of the materials examined in this work can change easily from the off-state to the on-state. This well-controlled ER characteristic was sensitive to the magnitude of $E$ and also 100% reversible. It was concluded that, due to enhanced ER response characteristic, applications of needle-like $TiO_2$/PRh/SO dispersion to controlled mechanical systems may be possible by taking advantage of the ER phenomenon. Similar response time behaviors were reported for nanosphere–$TiO_2$/PPy/SO and palygorskite/polyaniline/SO systems by Cabuk[24] and Chae *et al.*, respectively.[16]

### Effect of Shear Rate on Shear Stress and Viscosity

Figure 4(a,b) show the shear viscosity behaviors of needle-like $TiO_2$/SO and needle-like $TiO_2$/PRh/SO as functions of the shear rate, respectively. The shear thinning non-Newtonian viscoelastic behaviors were confirmed for $E = 0$ kV mm$^{-1}$ condition.

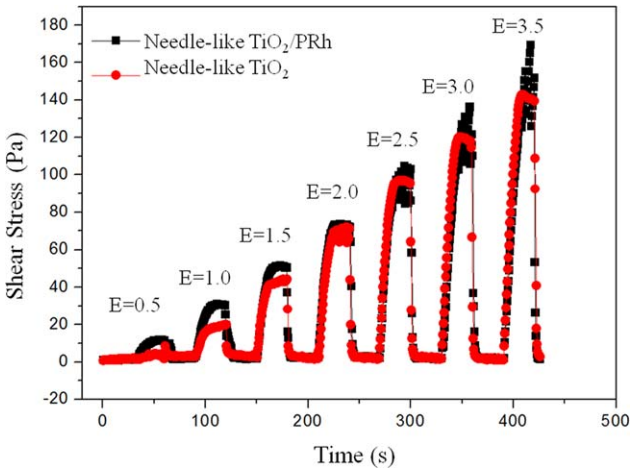


**Figure 3.** Change in shear stress with time (E = 0–3.5 kV $mm^{-1}$, $\varphi = 2.5\%$, $\dot{\gamma} = 1.0\ s^{-1}$). [Color figure can be viewed in the online issue, which is available at wileyonlinelibrary.com.]

Shear stresses of needle-like $TiO_2$/SO [Figure 4(c)] and needle-like $TiO_2$/PRh/SO [Figure 4(d)] systems also showed increases with rising shear rates and electric field strengths with yields as expected. It was observed that, needle-like $TiO_2$/PRh particles responded quickly to the external electric field stimuli by polarizing between the electrodes, due to the dipole–dipole interactions of the suspended particles, and formed fibrillar structures along the electric field direction and resulted with positive ER effect. In a study carried out by Cetin *et al.*, firstly observed negative ER effect (decrease of electric field induced viscosity) for the polyindene/colemanite/SO system were reported to be turned into the positive one after the inclusion of nonionic surfactant Triton X-100.[28]

These experimentally obtained shear rate–shear stress curves were also subjected to Cheng Hai Hong and Hyoung Jin Choi (CCJ) Model curve fittings with good agreements.[29]

$$\tau = \frac{\tau_y}{(1+(t_1\dot{\gamma})^{\alpha})} + \eta_{\infty}\left(1+\frac{1}{(t_2\dot{\gamma})^{\beta}}\right)\dot{\gamma} \qquad (8)$$

where $t_1$ and $t_2$ are time constants, $\dot{\gamma}$ is shear rate, $\tau_y$ is dynamic yield stress, $\eta_{\infty}$ is viscosity at high shear rate, $\alpha$ is related to the decrease in the stress, and $\beta$ is a constant in the range of $0 < \beta \leq 1$. This six parameter model explains the shear stress reduction in the low shear rate region and gives the $\tau_y$ values much more accuretly than the other models.

It is important to calculate the dynamic yield stresses of these suspensions under $E = 0$–3.5 kV $mm^{-1}$ conditions. To obtain the $\tau_y$ values, stress–strain measurements were conducted at

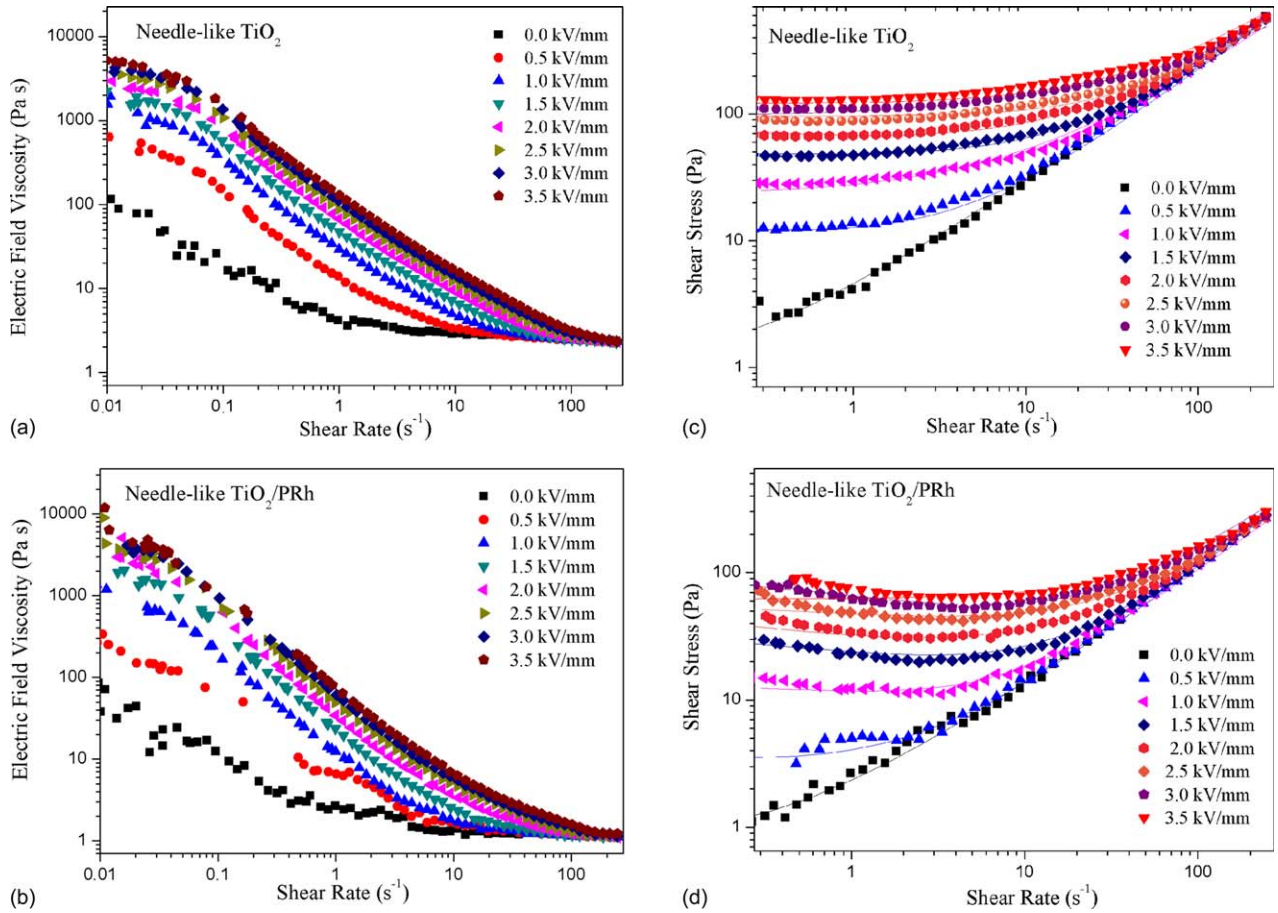


**Figure 4.** Effects of shear rates on viscosities and shear stresses of the materials ($T = 25°C$). [Color figure can be viewed in the online issue, which is available at wileyonlinelibrary.com.]

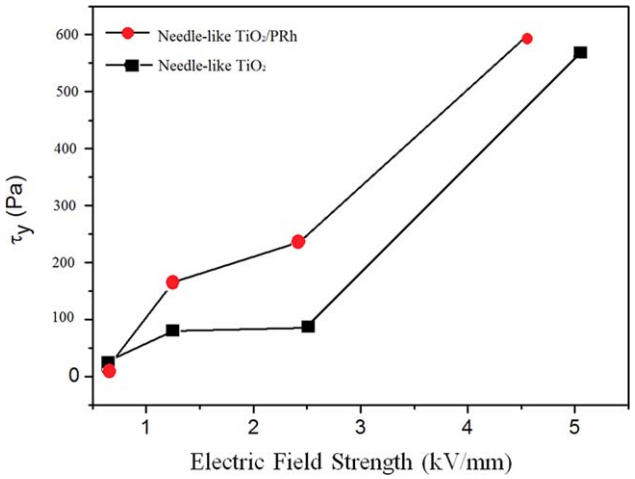


**Figure 5.** Changes in dynamic yield stresses with electric field strengths ($\varphi = 2.5\%$, $T = 25°C$). [Color figure can be viewed in the online issue, which is available at wileyonlinelibrary.com.]

very low shear rates, and the shear stress values at which the viscosities decrease suddenly are defined as the dynamic yield stresses. For this purpose, $\tau_y$ values of needle-like $TiO_2$/SO and needle-like $TiO_2$/PRh/SO systems calculated from shear rate–shear stress graphs at the volume fraction of $\varphi = 2.5\%$ and results obtained are depicted in Figure 5. Increasing $\tau_y$ values were observed for the both suspensions and highest $\tau_y$ values were obtained for needle-like $TiO_2$/PRh/SO and needle-like $TiO_2$/SO systems as 592 and 584 Pa, respectively under $E = 3.5$ kV $mm^{-1}$ and $\varphi = 2.5\%$ conditions. In an our previous study, increasing $\tau_y$ values were obtained with rising volume fractions for nanosphere–$TiO_2$/SO and nanosphere–$TiO_2$/PPy/SO systems and the highest $\tau_y$ values were obtained as 280 and 200 Pa, respectively under $E = 3.5$ kV $mm^{-1}$ and $\varphi = 5\%$ conditions.[24] Further, enhanced yield stress values were reported for polyindene/colemanite/SO system after the inclusion of nonionic surfactant Triton X-100.[26]

### Effect of Temperature on Shear Stress

Temperature is one of the important parameters to be explored for ER fluids. Temperature may affact the polarizability of an ER fluid depending on the changes on conductivity, dielectic constant and Brownian motions with rising temperature. To understand whether the pristine needle-like $TiO_2$/SO and needle-like $TiO_2$/PRh/SO systems have lost their ER strengths at low and elevated temperatures, changes in their shear stress values were investigated as a function of temperature (Figure 6). Shear stresses of needle-like $TiO_2$/SO and needle-like $TiO_2$/PRh/SO systems were observed to increase from 98 to 110 Pa and from 100 to 127 Pa, respectively which correspond to a shear stress or ER gains of 12 and 27 Pa between 10 and 70°C. Enhancements of shear stress values at elevated temperatures were attributed to the increased electrical conductivity and enhanced interfacial polarization as a result of the increased mismatch in conductivity between the two phases of the ER fluid in a study carried out on polyaniline/K-feldspar conducting composite by Ozlem *et al.*[30] This may also be attributed to the trace amount of adsorbed water by the ER suspensions which cause the polarizations of electrical double layers and forms bridges between the suspended particles.

### Effect of Frequency on Storage Modulus

To determine the vibration damping and dynamic viscoelastic properties of needle-like $TiO_2$/SO [Figure 7(a)] and needle-like $TiO_2$/PRh/SO ER systems [Figure 7(b)], effects of angular frequency on storage ($G'$) modulus in linear viscoelastic region (LVR) were investigated. $G'$ values of needle-like $TiO_2$/PRh/SO ER system were observed to slightly increase with rising frequencies up to approximately 10 Hz and then levelled off whereas, no increments were observed on $G'$ values of needle-like $TiO_2$/SO system with the influence of frequency. On the other hand, higher electric field induced storage moduli data were recorded with increments under electric field strengths for the both materials examined which indicates their solid-like behaviors and electric field stimulus storage capabilities. The frequency-independent behavior of $G'$ of the hybrid nanocomposite may be attributed to the anisotropic alignment of suspended particles in a 3D microstructure with the influence of the induction of external $E$.[31] Generally, colloidally stable dispersions form 3D network structures due to the electric field induced intermolecular interactions. Polarizabilities and relaxation times of $TiO_2$ nanoparticles also depend on their geometries as well as nature of the shell materials used for their hybridization which was also supported by the storage and loss moduli behaviors of nanosphere–$TiO_2$/PPy/SO system.[24]

### Effect of Time on Storage Modulus

To identify the changes in storage modulus in time is important for a viscoelastic material interms of their shelf lives and end-use applications. For this purpose, effect of $E$ on time on storage moduli of needle-like $TiO_2$/SO [Figure 8(a)] and needle-like $TiO_2$/PRh/SO systems [Figure 8(b)] were investigated. It was observed that storage moduli of the both systems rose with the increments upon the applications of $E$ but remained stable in time durations, without showing any ER strength losses, which is a desired property for potential industrial applications. These behaviors indicate that needle-like $TiO_2$ and needle-like $TiO_2$/PRh hybrid systems are able to perceive $E$ by the strengthened electric field induced

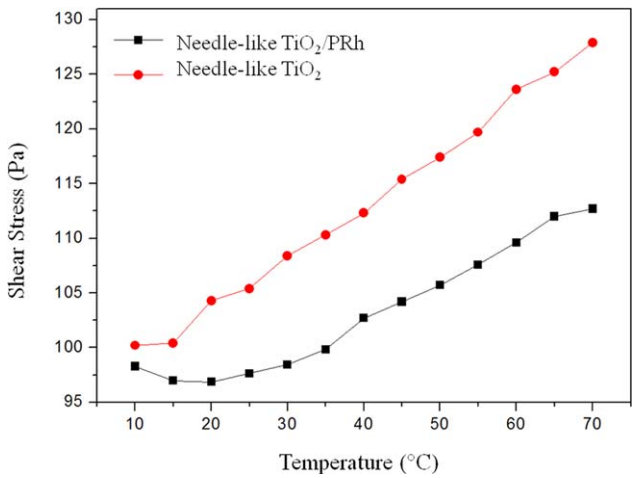


**Figure 6.** Effect of temperatures on shear stresses ($\varphi = 2.5\%$, $E = 2$ kV $mm^{-1}$, $\dot{\gamma} = 1\ s^{-1}$). [Color figure can be viewed in the online issue, which is available at wileyonlinelibrary.com.]

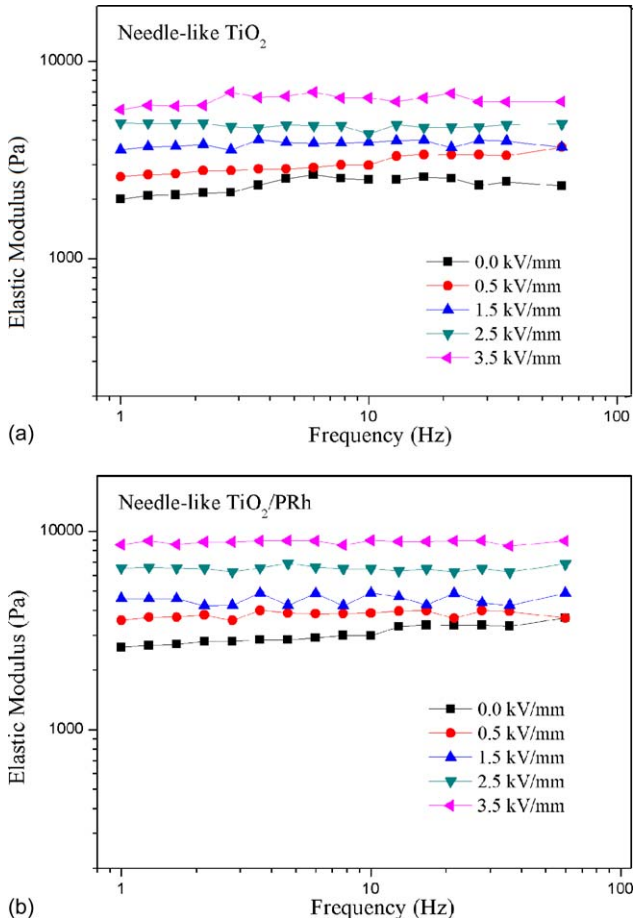


**Figure 7.** Effect of frequency on storage and loss moduli ($\dot{\gamma} = 1.0\ s^{-1}$, $\varphi = 2.5\%$, $T = 25°C$). [Color figure can be viewed in the online issue, which is available at wileyonlinelibrary.com.]

intermolecular interactions, acted as smart materials, and significantly showed the vibration damping capacity. Similar smart material behavior was reported in the study carried out on polythiophene/borax/SO system.[32]

## CREEP AND CREEP-RECOVERY RESULTS

The creep and creep–recovery tests provide important information regarding the viscoelastic properties of needle-like $TiO_2$/PRh/SO system. A typical creep–recovery curve composes of the instantaneous strain $\gamma_s(t)$, retarded elastic strain $\gamma_d(t)$, and the viscous strain $\gamma_v(t)$ or irreversible component of the strain. When a constant stress is applied to a viscoelastic material for a time period of t, time dependent creep-strain $\gamma_c(t)$, may be expressed as:

$$\gamma_c(t) = \gamma_s(t) + \gamma_d(t) + \gamma_v(t) \quad (9)$$

Time dependent deformations may be recovered when the applied stress is removed ($\tau = 0$ Pa). Flow curve of a viscoelastic material shows two regions under a constant temperature, namely creep phase and creep–recovery phase, which is typically shown on the inset of Figure 10. When the applied stress was set to $\tau = 0$ Pa, instantaneous elastic response ($\gamma_e$) was recovered immediately and delayed elastic response ($\gamma_d$) was recovered gradually. That is why, the time dependent recovered strain ($\gamma_R$(t)) is given by:

$$\gamma_R(t) = \gamma_e + \gamma_d(t) \quad (10)$$

Creep tests were carried out at two different stages. In one of them instantaneous constant stress was applied ($\tau = 30$ Pa) to needle-like $TiO_2$/PRh/SO system under isothermal ($T = 25°C$) and various external electric field conditions ($E = 0$–$3.5$ kV mm$^{-1}$) and increases in strains were measured as a function of time (Figure 9). In the other experiment, varying shear stresses were applied to the material under isothermal ($T = 25°C$) and constant electric field ($E = 3.5$ kV mm$^{-1}$) conditions (Figure 10). During the recovery tests, applied stress was removed ($\tau = 0$ Pa) and percentage recoveries ($R$ %) of sometime dependent deformations of the material were calculated using eq. (11):

$$\text{Recovery}\ (\%) = \frac{\gamma_i - \gamma_f}{\gamma_i} \times 100 \quad (11)$$

where $\gamma_i$ is the total strain acquired before removing the applied stress and $\gamma_f$ is the average steady state strain after removing the applied stress. Percentage recoveries ($R_E$) under $\tau = 30$ Pa and varying electric field strengths were determined to be in the following order: $R_E = 1.5 = 83\% > R_E = 2.5 = 72\% > R_E = 3.5 = 68\%$. On the other hand, change in the percentage recoveries ($R_\tau$) with changing shear stresses were determined to be in the following

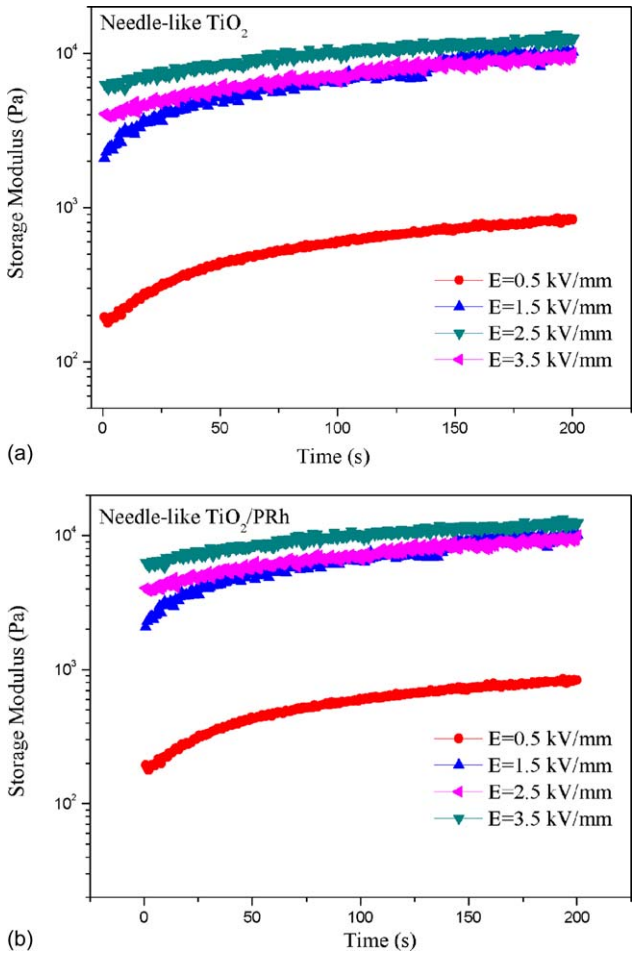


**Figure 8.** Effect of time on storage and loss moduli ($\dot{\gamma} = 1.0\ s^{-1}$, $\varphi = 2.5\%$, f = 1 Hz, $T = 25°C$). [Color figure can be viewed in the online issue, which is available at wileyonlinelibrary.com.]

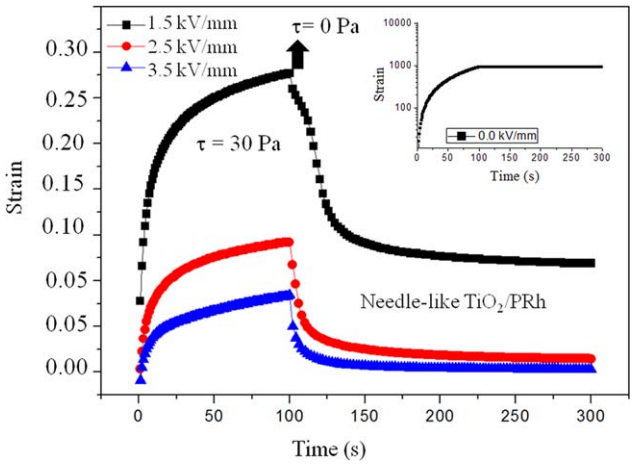


**Figure 9.** Creep–recovery response for needle-like $TiO_2$/PRh/SO suspension ($\hat{o} = 30$ Pa, $\varphi = 5\%$, $T = 25°C$). Inset shows $E = 0$ condition. [Color figure can be viewed in the online issue, which is available at wileyonlinelibrary.com.]

order: $R_{\tau=20\ Pa} = 63\% < R_{\tau=30\ Pa} = 68\% < R_{\tau=40\ Pa} = 76\% < R_{\tau=60\ Pa} = 88\%$. It was demonstrated that percentage recoveries of needle-like $TiO_2$/PRh/SO system decreased with increasing $E$ and increased with rising shear stresses by demonstrating that the system is a smart one and has a capacity to store some of the deformations by polarising the needle-like particles between the electrodes and forming stronger anisotropic chains. In a study carried out on creep−recovery behaviors of core−shell-structured monodisperse copolymer/silica/SO based ER fluid by Liu *et al.*, 60 and 93% recoveries were reported under $\tau = 10$ Pa, $E = 1$ and $E = 2$ kV $mm^{-1}$ conditions, respectively and viscoelastic time dependent deformations were reported both for the creep and recovery phases.[33] Also, in a study carried out on creep–recovery behavior of polyaniline based ER fluid by Cho *et al.*, increased strain recovery with rising $E$ was reported.[34] In another study carried out in our laboratory creep–recovery of nanosphere–$TiO_2$/SO and nanosphere–$TiO_2$/PPy/SO systems were observed to be 34 and

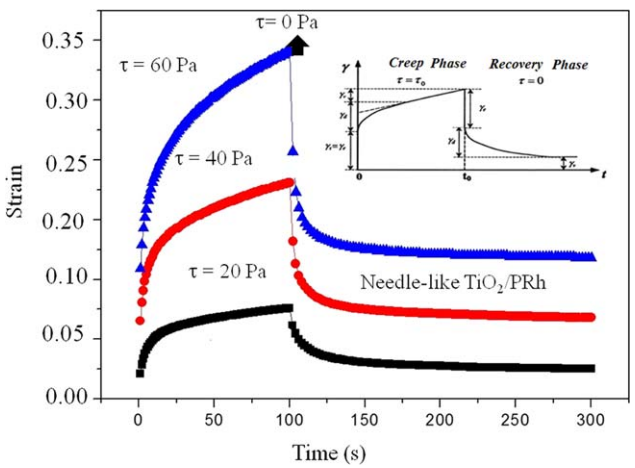


**Figure 10.** Creep–recovery response for needle-like $TiO_2$/PRh/SO suspension ($\hat{o} = 20$, 40, 60 Pa; $\varphi = 2.5\%$, $T = 25°C$). Inset shows typical creep–recovery curve. [Color figure can be viewed in the online issue, which is available at wileyonlinelibrary.com.]

64%, respectively under $\tau = 5$ Pa, $E = 3.5$ kV $mm^{-1}$, and $T = 25°C$ conditions. It was concluded that, these materials behave as smart ones by storing the deformations in their structures and may be used for potential industrial vibration damping applications. Enhanced creep–recovery behaviors are reported in the literature by Cetin *et al.*, for colemanite/polyindene/SO system after the inclusion of Triton X-100.[26,28]

## CONCLUSIONS

Facile fabrication of core/shell structured nanoparticles composed of needle-like $TiO_2$ and polyrhodanine as a new smart material was carried out with enough colloidal stability, good dielectric properties, short and reversible response time, and high yield stress. Elevated temperatures observed to enhance the ER activity of the suspensions due to easily polarizable geometry of suspended needle-like $TiO_2$ particles. Dynamic viscoelastic measurements revealed that storage moduli of needle-like $TiO_2$/PRh/SO and needle-like $TiO_2$/SO systems were bigger than the viscous moduli values and this was dominant for the latter. Both materials showed viscous behavior when no electric field was applied during creep–recovery measurements, but behaved as non-Newtonian smart materials under $E$ and resistant to high shear stresses by indicating that they are good candidates for potential industrial vibration damping applications.

## ACKNOWLEDGMENTS

The authors are grateful to the Turkish Scientific and Technological Research Council (111 T 637) and COST Action CM1101 for the support of this study.

## REFERENCES

1. Chen, X.; Mao, S. S. *Chem. Rev.* **2007**, *107*, 2891.
2. Ozkan, S.; Unal, H. I.; Yılmaz, E.; Suludere, Z. *J. Appl. Polym. Sci* **2015**, *132*, 41554.
3. Shen, L.; Zhang, X.; Li, H.; Yuan, C.; Cao, G. *J Phys. Chem. Lett.* **2011**, *2*, 3096.
4. Kumar, N.; Hazarika, S. N.; Limbu, S.; Boruah, R.; Namsa, N. D.; Das, S. K. *Micropor. Mesopor. Mat.* **2015**, *213*, 181.
5. Tan, L. H.; Xing, H.; Lu, Y. *Acc. Chem. Res.* **2014**, *47*, 1881.
6. Charbonneau, C.; Holliman, P. J.; Davies, M. L.; Watson, T. M.; Worsley, D. A. *J. Colloid Interface Sci.* **2015**, *442*, 110.
7. Verenovski, N.; Andreozzi, P.; La Mesa, C.; Sfiligoj-Smole, M. *Surf. Coat. Tech.* **2010**, *204*, 1445.
8. Plachy, T.; Mrlik, M.; Kozakova, Z.; Suly, P.; Sedlacik, M.; Pavlinek, V.; Kuritka, I. *ACS Appl. Mater. Interfaces* **2015**, *7*, 3725.
9. Zhang, Y. G.; Ma, L. L.; Li, J. L.; Yu, Y. *Environ. Sci. Technol.* **2007**, *41*, 6264.
10. Liu, Y. D.; Zhang, K.; Zhang, W. L.; Choi, H. J. *Aust. J. Chem.* **2012**, *65*, 1195.
11. Shen, R.; Wang, X.; Lu, Y.; Wang, D.; Sun, G.; Cao, Z.; Lu, K. *Adv. Mater.* **2009**, *21*, 4631.
12. Wu, J.; Xu, G.; Cheng, Y.; Liu, F.; Guo, J.; Cui, P. *J. Colloid Interf. Sci.* **2012**, *378378*, 36.

13. Plachy, T.; Sedlacik, M.; Pavlinek, V.; Stejskal, J. *J. Mater. Chem. C* **2015**, *3*, 9973.
14. Crippa, M.; Bianchi, A.; Cristofori, D.; D'Arienzo, M.; Merletti, F.; Morazzoni, F.; Scotti, R.; Simonutti, R. *J. Mater. Chem. C* **2013**, *1*, 484.
15. Krysiak, E.; Wypych-Puszkarz, A.; Krysiak, K.; Nowaczyk, G.; Makrocka-Rydzyk, M.; Jurga, S.; Ulanski, J. *Synth. Met.* **2015**, *209*, 150.
16. Chae, H. S.; Zhang, W. L.; Piao, S. H.; Choi, H. *J. Appl. Clay Sci.* **2015**, *107*, 165.
17. Choi, H. J.; Cho, M. S.; Kim, J. W. *Korea Aust. Rheol. J.* **2001**, *13*, 197.
18. Shin, K.; Kim, D.; Cho, J. C.; Lim, H. S.; Kim, J. W.; Suh, K. D. *J. Colloid Interf. Sci.* **2012**, *374374*, 18.
19. Wahed, A. K. E.; Sproston, J. L.; Stanway, R. *J. Phys. D: Appl. Phys.* **1998**, *31*, 2964.
20. Lee, S.; Cho, M. S.; Choi, H. J. *Polymer* **2005**, *46*, 1317.
21. Koyuncu, K.; Unal, H. I.; Gumus, O. Y.; Erol, O.; Sari, B.; Ergin, T. *Polym. Adv. Technol.* **2012**, *23*, 1464.
22. Li, W. H.; Du, H.; Chen, G.; Yeo, S. H. *Mater. Sci. Eng. A: Struct.* **2002**, *333*, 368.
23. Sari, B.; Yavas, N.; Makulogullari, M.; Erol, O.; Unal, H. I. *React. Funct. Polym.* **2009**, *69*, 808.
24. Cabuk, S.; Unal, H. I. *React. Funct. Polym.* **2015**, *95*, 1.
25. Cole, K. S.; Cole, R. H. *J. Chem. Phys.* **1941**, *90*, 341.
26. Wei, C.; Zhu, Y.; Jin, Y.; Yang, X. *Mater. Res. Bull.* **2008**, *43*, 3263.
27. Kawai, A.; Ide, Y.; Inoue, A.; Ikazaki, F. *J. Chem. Phys.* **1998**, *109*, 4587.
28. Cetin, B.; Unal, H. I.; Erol, O. *Smart Mater. Struct.* **2012**, *21*, 125011.
29. Cho, M. S.; Choi, H. J.; Jhon, M. S. *Polymer* **2005**, *46*, 11484.
30. Erol, O.; Karakisla, M.; Unal, H. I.; Sacak, M. *J. Compos. Mater.* **2012**, *46*, 1295.
31. Sumita, I.; Manga, M. *Earth Planet Sci. Lett.* **2008**, *269269*, 468.
32. Gumus, O. Y.; Unal, H. I.; Erol, O. *Polym. Compos.* **2011**, *32*, 756.
33. Liu, Y. D.; Quan, X.; Hwang, B.; Kwon, Y. K.; Choi, H. J *Langmuir* **2014**, *30*, 1729.
34. Cho, M. S.; Lee, J. H.; Choi, H. J. *J. Mater. Sci.* **2004**, *39*, 1377.